Available online at www.sciencedirect.com
SCIENCE DIRECT®

Journal of the European Ceramic Society 24 (2004) 239–246

www.elsevier.com/locate/jeurceramsoc

Manufacturing of a gear wheel made from reaction bonded alumina—numerical simulation of the sinterforming process

M. Reiterer*, T. Kraft, H. Riedel

Fraunhofer-Institute for Mechanics of Materials; Wöhlerstr. 11, D-79108 Freiburg, Germany

Abstract

Sinter forming is a recently developed process for the production of advanced ceramic components. It combines pressure-supported sintering and superplastic deformation, and allows RBAO (Reaction Bonded Alumina) to be sintered without grain coarsening due to the reduction of process time and dwell temperature. Thus, sinterforming can achieve near net shaping and defect free components for highly stressed applications. As many phenomena interact during sinter forming, the process parameters for producing complex shaped parts are difficult to identify without numerical tools. Therefore, a micromechanical model for solid state sintering has been used to investigate the process. The model was extended to consider source controlled diffusion in order to describe the non-linear stress/strain dependence. Several experiments were made in order to determine the material parameters of the model. The model has been implemented as a user subroutine in ABAQUS/Explicit® and is validated by numerical simulations of the accomplished experiments. To show the possibilities of the finite element simulation, the sinter forming process is numerically carried out for a RBAO gear wheel.

Keywords: Hot pressing; RBAO; Simulation; Sintering

1. Introduction

Innovative and powerful materials are an important key for the realisation of 21st century technologies. Presently materials are validated not only by their abilities, but production costs and environmental sustainability are factored in as well. In respect to their technical properties ceramics meet the demands well. However, due to the high processing costs this group of materials is still not competitive in many applications. The most expensive production step is the mechanical finishing which is unavoidable especially for components of complex geometry. That is the reason why a near net shape technology for the fabrication of ceramic parts is desirable as, for example, sinter forming. This process, which was recently developed for Reaction Bonded Alumina (RBAO) at the TU Hamburg-Harburg,[1] seems to be suitable for high-strength and corrosion-resistant components.

The technique of producing RBAO was introduced in the late eighties.[2] In this manufacturing route Al and Al_2O_3 powders are milled together in an organic liquid, dried in air, sieved and pressed to green bodies. A thermal treatment of the semi-finished product in air leads to pure alumina since the Al particles are oxidised. The wet milling is the central step, which determines the efficiency of the oxidation process and the properties of the final product.[3,4] Extensive studies concerning the oxidation process are presented in.[5–7]

As RBAO consolidates via solid-state sintering, the gas pressure in the pores prevents the reaching of full density, if the samples are free sintered. An application of external stress, i.e. by HIP, promotes the sinter process and increases the final density. Ventakatachri and Raj[8] reported that flattening of pores due to shear stress, which is induced by sinter forging, is a very effective method of eliminating defects and a significant enhancement of strength was obtained. By doping RBAO with ZrO_2 undesired grain coarsening is prevented and the ability of plastic deformation can be increased.[2] The materials used here show a superplastic like behaviour for grain diameters less than 1 μm and temperatures between 1250 and 1450 °C.[1] Generally,

* Corresponding author. On leave from: Department of Structural and Functional Ceramics, University of Leoben, Peter-Tunner-Straße 5, A-8700 Leoben, Austria.
E-mail address: reit@iwm.fhg.de (M. Reiterer).

0955-2219/03/$ - see front matter © 2003 Elsevier Ltd. All rights reserved.
doi:10.1016/S0955-2219(03)00240-1

superplastic deformation in tension was observed first for ceramics by Wakai et al.[9] in 1986.

In contrast to superplastic deformation of dense semi-finished products, porous parts, which are compacted and deformed simultaneously, are used for sinter forming. (If sinter forging is performed in a closed die, to achieve near-net-shaped components, it is frequently called sinter forming.) There are numerous advantages of this new procedure: as the process starts with the porous material, the deformation rate is higher than in the case of an already dense material. Because of the reduction of process time and the application of load, defect-free and fine-grained microstructures can be achieved even for materials without liquid-phase sintering.[10,11] At the later stage of the process, the material is in contact with the die, and hence, the quality of the surface is only restricted by the accuracy of the tools.

Many phenomena contribute to this compaction and deformation procedure and interact physically. Therefore, the required process parameters are difficult to identify, and the use of numerical simulations is reasonable to find optimised manufacturing conditions.

2. A micromechanical model for sinter forming

To simulate sinter forming, several approaches are thinkable: Gurson-type models, which describe the growth and shrinkage of pores depending on the stress state, have the disadvantage that time dependent processes are not considered, which are typical for sinter forming. Purely phenomenological sintering models like Abouaf et al.[12]—see also the review of Olevsky[13]—are principally restricted in their predictability. Therefore, a physically based solid state sintering model, which was developed mainly by Riedel and Svoboda,[14–17] was chosen. A detailed summary is given in this issue[18] or in.[19]

The concept of the model is based on the work of Ashby[20,21] as far as sintering mechanisms are concerned and on that of Jagota and Dawson[22] and McMeeking and Kuhn[23] as relates to the mechanical aspects. Solid state sintering of ceramics at low pressure takes place by grain boundary, surface and volume diffusion.

The constitutive equation is expressed as a relation between the macroscopic strain rate tensor and the stress tensor:

$$\dot{\varepsilon}_{ij} = \frac{\sigma'_{ij}}{2G} + \delta_{ij}\frac{\sigma_m - \sigma_s + \Delta p}{3K} \tag{1}$$

where σ'_{ij} is the stress deviator, σ_m is the hydrostatic stress, Δp is a gas overpressure which may develop in closed pores, δ_{ij} is the Kronecker symbol, G and K are shear and bulk viscosity, respectively, and σ_s is the sinter stress which arises from the surface tension forces of the pores. The sintering model[18] takes into account diffusive transport of matter and grain coarsening, and it uses models for open and closed porosity. Since this transition is continuous, a numerical interpolation is applied.

In its original form the model leads to a linear stress/strain–rate relation, i.e. K and G are independent of the stress. Various authors[1,24–26] find a non linear stress/strain relation for oxide ceramics when they are deformed at elevated temperatures and stresses between 5 and 100 MPa. Berbon and Langdon[27] suggest a reasonable explanation of this behaviour in compression tests for superplastic 3Y-ZTP, which seems to be applicable here as well. They assume, that the grain boundaries do not act like perfect sources and sinks for vacancies in respect to diffusion. Consequently, the nucleation of vacancies is the rate controlling effect. This mechanism is called "Source Controlled Diffusion" or "Interface Reaction-Controlled Diffusion" and increases as grain size decreases.[28,29] To consider this mechanism, the viscosities are expressed as quadratic terms:

$$G = G_{\text{lin}}\left(1 + \frac{\alpha}{\bar{\sigma}R^2}\right) \tag{2}$$

$$K = K_{\text{lin}}\left(1 + \frac{\alpha}{\bar{\sigma}R^2}\right) \tag{3}$$

with the linear viscosities, G_{lin} and K_{lin}, from[18] and a correction due to source controlled diffusion. Here α is a free parameter, R is the grain radius, and $\bar{\sigma}$ is an effective stress given by:

$$\bar{\sigma} = \tfrac{1}{2}\left|\sigma_m - \sigma_s + \Delta p\right| + \tfrac{1}{2}\sigma_e \tag{4}$$

where σ_e is the von Mises equivalent stress. Due to the introduction of terms for source controlled diffusion, it can be expected that sinter simulations of materials with very fine microstructure achieve better results, even for pressureless processes.

3. Material properties and sinter forming experiments

3.1. Material properties

In order to obtain good formability, grain growth of RBAO has to be suppressed, which can be reached by adding ZrO_2.[2] Therefore, 20 vol.% 2Y-ZTP was milled together with 44 vol.% Al and the 36 vol.% Al_2O_3 powder in an organic liquid. This material will be referred to as pure RBAO in this work. The dried powder was uniaxially pressed and subsequently oxidised in air at raising temperatures between 350 and 800 °C. Four-point-bending tests of the sinter formed material showed a strength of 1050 MPa and a fracture toughness of 3.5 $MPam^{1/2}$.

In order to reduce the sinter forming temperature, 2% CuO and 2% TiO_2 were added to the zirconia toughened RBAO.[30,31] This powder is named doped RBAO here. A decrease in strength ($\sigma_{4PB} = 500$ MPa) was accompanied by a lower processing temperature and a higher fracture toughness of 5 $MPam^{1/2}$. The reasons for this significant loss in strength are currently being investigated.

3.2. Sinter forming of cylinders

Several sinter forming experiments of cylindrical samples were performed at different stresses and sinter temperatures on pure and doped RBAO. The previously reaction bonded samples were provided by the TU Hamburg-Harburg. Presintered specimens with a height of 10 mm and a diameter of 8 mm were placed in the sinter forming device, which is also known as load dilatometer. The furnace was heated up to sinter forging temperature at a rate of 10 K/min, and the samples were loaded with different axial stresses, which had been applied for 60–150 min. The axial load σ_z is applied within 300 s after reaching the maximum temperature. Axial force, height and diameter were recorded during the experiments.

The development of the logarithmic strain of height and diameter of the samples, which were used later for fitting the model parameters, are shown in Fig. 1. The experiments with pure material (a) were performed at a sinter forming temperature T_{SF} of 1450 °C and axial stresses σ_z between 5 and 30 MPa. The specimens made from doped RBAO (b) were exposed to a temperature of 1150 °C and σ_z ranged from 5 to 20 MPa. The upper branches of the plots represent the radial and the lower branches the axial strains.

The influence of the axial load on the compression behaviour of the samples is shown in Fig. 2. The applied way of density calculation by estimating a barrel shape of the samples is not proper for precise validations, but was used to demonstrate the influence of different axial stresses and compare the experimental and numerical results. Measuring errors and deviations from the supposed shape can lead to a relative mean density of slightly more than 100%. The higher the axial stress is,

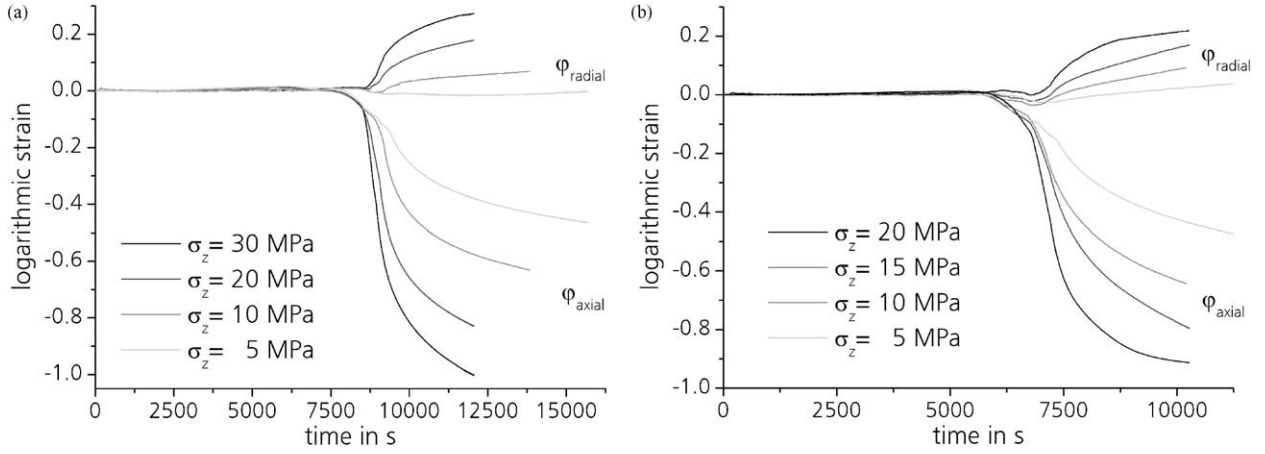

Fig. 1. Development of logarithmic strain of height and diameter. The samples are made from pure RBAO, $T_{SF} = 1450$ °C, (a) and doped RBAO, $T_{SF} = 1150$ °C, (b).

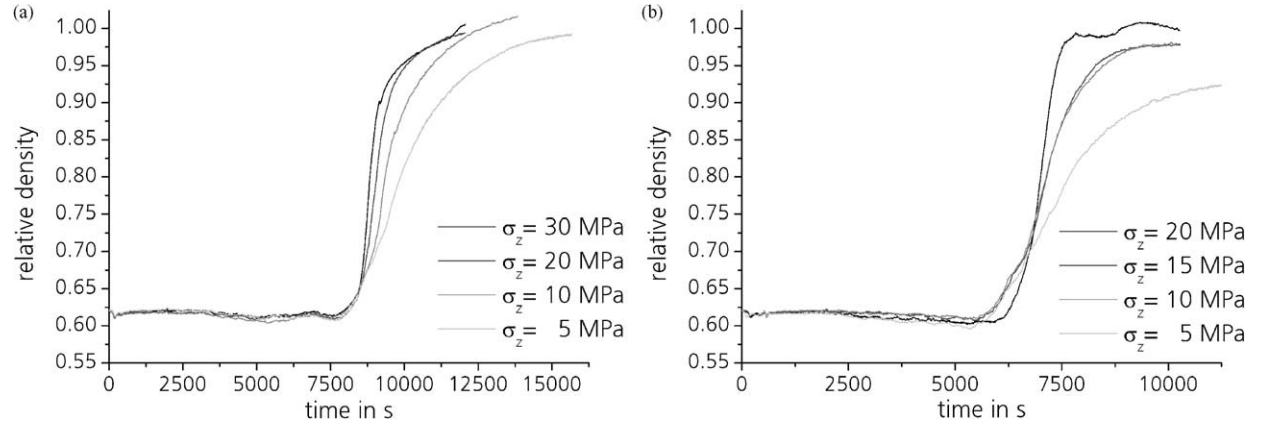

Fig. 2. Density increase during sinter forming for pure (a) and doped (b) RBAO.

the more steeply the density curve rises. In order to balance the lower sinter activity and to achieve high densities, the dwell time at lower stresses was elongated. However, the axial stress of 5 MPa seems to be too low for both types of materials.

4. Identification of the model parameters

A PC-FORTRAN program, which describes the behaviour of an axisymmetric element during sinter forming, was developed for determining the model parameters. The parameters were identified by adjusting the evolution of density, strains and grain size to the experimental results. The most important influences derive from the activation energy and the pre-exponential factors of the three different diffusion mechanisms and the grain growth kinetics. Additionally, the model depends on grain boundary and surface energy.

Fig. 3 shows the development of the logarithmic strains in radial and axial direction for an axial stress of 20 MPa and doped RBAO. The solid lines represent the experimental results and the dotted lines are the numerical results obtained for a parameter set fitted to all experiments. Sintering starts earlier in the experiment than in the simulation as the powder has a bimodal grain size distribution due to the production route. For the simulation, an average grain size is assumed, since the model presently considers only a monomodal distribution.

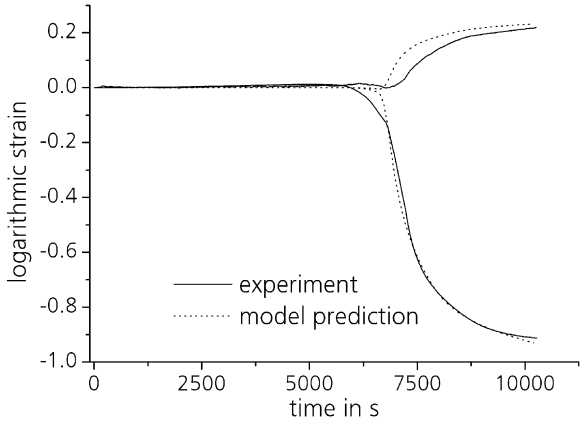

Fig. 3. Development of logarithmic strain of height and diameter. The sample is made from doped RBAO and an axial stress of 20 MPa.

The difference of the axial and radial strain of several experiments is plotted in Fig. 4. Densification and deformation depend significantly on the axial stress and are predicted very successfully by the model. The parameters for both materials are given in Table 1. External gas pressure, initial density and grain size are taken from the experimental data. The other coefficients lie, as far as known, within a physical meaningful range.

Table 1
Parameters for the model of sinter forming of pure and doped RBAO. (the parameters are defined in Ref.[18])

Parameter	symbol	Pure RBAO	Doped. RBAO
Initial relative density	ρ_0	0.62	0.62
Initial grain radius	R_0	0.1 μm	0.05 μm
External gas pressure	p_{ex}	0.1 MPa	0.1 MPa
Molecular volume	Ω	1.42e-26 m^3	1.42e-26 m^3
Grain boundary diffusion	δD_b^0	1.75e-10 m^3/s	1.0e-7 m^3/s
	Q_b	490 000 J/mol	430 000 J/mol
Surface diffusion	δD_s^0	1.70e-10 m^3/s	3.0e-7 m^3/s
	Q_s	490 000 J/mol	430 000 J/mol
Volume diffusion	D_v^0	1.0e+9 m^2/s	1.0e+6 m^2/s
	Q_v	800 000 J/mol	680 000 J/mol
Grain boundary mobility	$\gamma_b M_{b0}/4$	1.0e-5 m^2/s	4.5e-4 m^2/s
	Q_m	480 000 J/mol	437 000 J/mol
Surface energy	γ_s	0.75 J/m^2	0.75 J/m^2
Dihehdal angle	ψ	60 °	60 °
Initial deviation of the Hillert grain size distribution	δ	0.5	0.5
Pore detachment	β_0	1.0	1.0
G/K for open porosity	β_1	0.243	0.216
Multiplier for G/K at closed porosity	β_2	0.9	0.8
Source-controlled diffusion	α	5.5e-8 N	5.0e-8 N

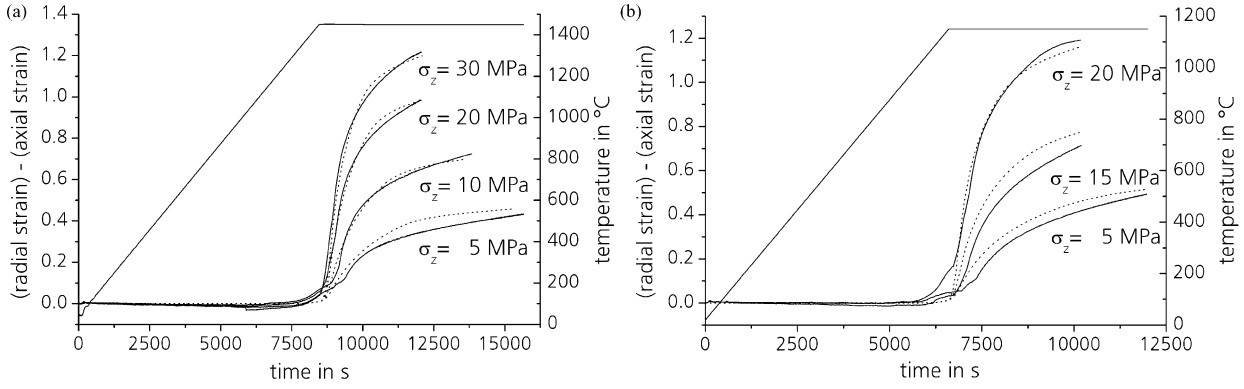

Fig. 4. Stress dependence of the strain rate (a: pure RBAO, b: doped RBAO). The axial load σ_z is applied within 300 s after reaching the maximum temperature. Dotted curves: numerical results; Solid lines: experiments.

5. Application of the model for simulations of sinter forming

5.1. Finite element simulation of sinter forming of cylinders

For the implementation of the material model the finite element code ABAQUS/Explicit® was selected, as it has advantages for 3D contact problems and large element distortions. The equations of the axisymmetric FORTRAN program had to be formulated in 3D components notation for the use in the materials subroutine VUMAT.

Axisymmetric finite element simulations were performed in order to verify the implementation of the model in the ABAQUS subroutine. Similar to the experiment, the calculation was performed "force controlled". The following plots show the original and deformed mesh (Fig. 5) and the relative density distribution at the end of the simulation (Fig. 6). The external conditions were the same as described in Fig. 1. As expected, a quite homogeneous distribution was

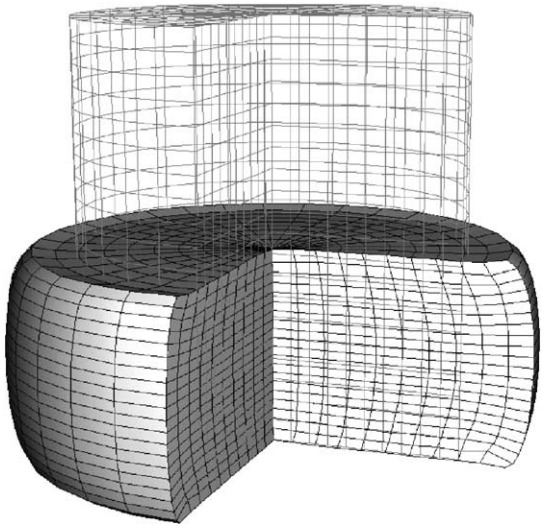

Fig. 5. Original and deformed mesh of a cylindrical sample made from doped RBAO. The load ($\sigma_z = 20$ MPa) was applied for 60 min at a temperature of 1150 °C and the friction coefficient is $\mu = 0.1$.

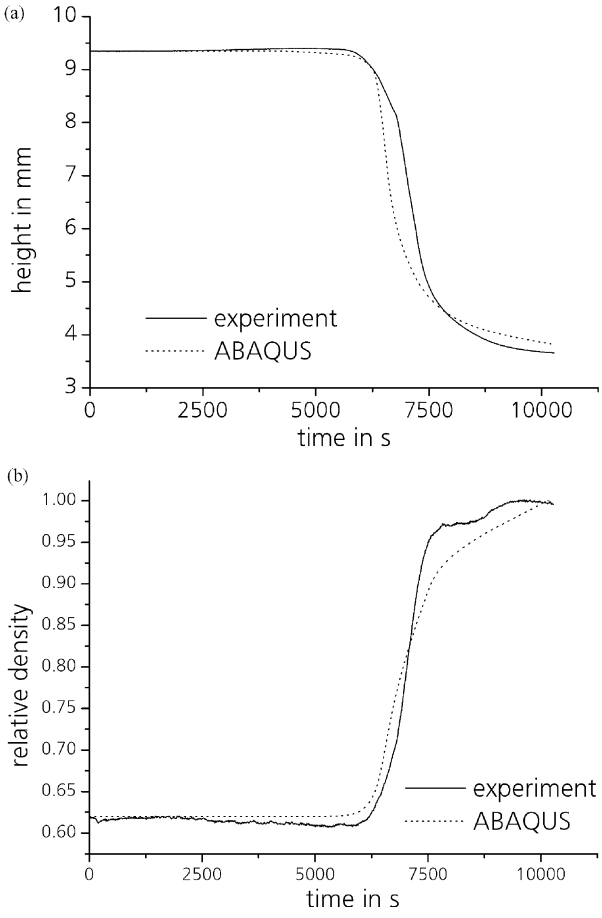

Fig. 7. Comparison between experiment and FE simulation (doped RBAO, $T_{SF} = 1150$ °C, $\sigma_z = 20$ MPa, $t = 60$ min). Evolution of height (a); Evolution of density (b).

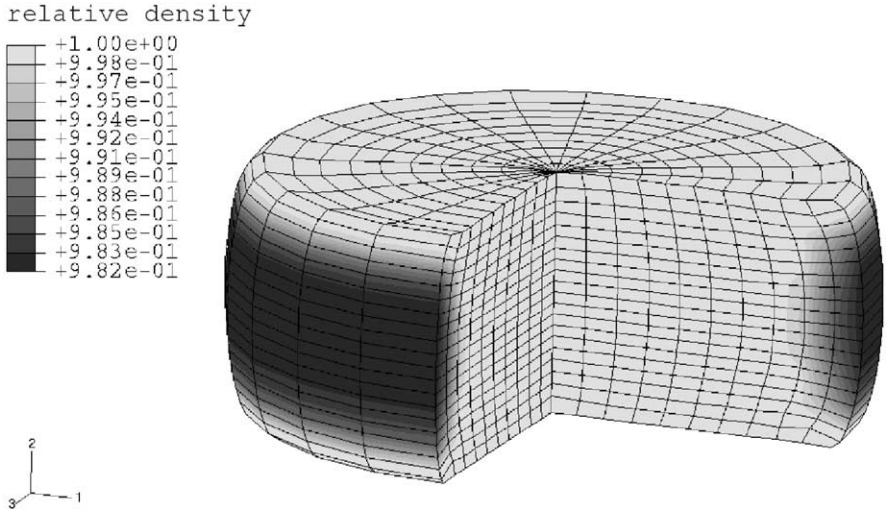

Fig. 6. Relative density of a sample after sinter forming. Only where tensile stresses are predominant, full density was not reached (details see Fig. 5).

Fig. 8. Sinter formed gear (diameter 35 mm) and tooling (die and punch) made of SiC.

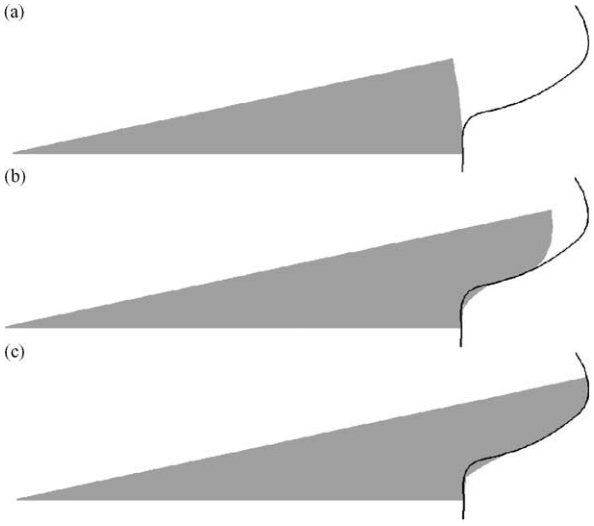

Fig. 9. Original shape (a), after 50% of t_{SF} (b) and final shape (c) of specimen and die.

obtained, with its minimum at the middle of the outline. A friction coefficient μ of 0.1 was estimated for the calculations, since for this value a good accordance with the outline of the experimental sample could be reached.

As soon as the load was applied the sample immediately decreased its height. Again a barrel shape was assumed to estimate the volume of the sample, which was used to calculate the evolution of the average density. The evolution of height and density is plotted in Fig. 7.

5.2. FE simulation of sinter forming of a gear wheel

To show the possibilities of the model, the manufacturing process of a gear wheel, which was sinter formed at the TU Hamburg-Harburg, was simulated. This demonstration part was chosen, as it has a high potential for early industrial applications. The die and the punch were made from SiC by ultra sonic erosion (Fig. 8). The white gear in front is the sinter formed component. The FE calculations will support the experimental work by determining the ideal geometry of the semi-finished product and optimal process conditions, e.g. the necessary temperature and pressure schedules to obtain a short production time without getting an undesired microstructure. Sinter forming of the gear wheel is numerically challenging as large element distortions occur at the tooth root surface.

For this calculation the material parameters of doped RBAO were used. The simulation started at a temperature of 800 °C and the heating rate was 10 °C/min. After reaching the maximum temperature of 1150 °C an axial stress of 60 MPa was applied. For the friction coefficient a value of 0.1 was used. Due to symmetrical reasons only a small section of the upper half of the component had to be simulated. The specimen and the die are

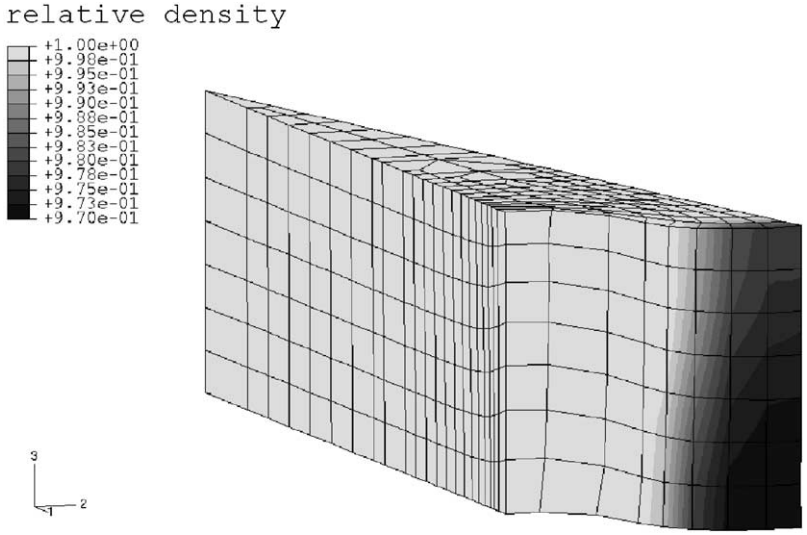

Fig.10. Density distribution of the gear wheel after 50% of the sinter forming time (doped RBAO, $T_{SF}=1150$ °C, $t_{SF}=90$ min, $\sigma_z=60$ MPa).

drawn at three different steps of the sinter forming process in top view (Fig. 9). The final shape arises as the material is pressed against the die and fills the cavity.

The tooth of the gear is already formed well and the densification process is nearly completed after 50% (90 min) of the dwell time (Fig. 10). According to the model, the figure shows that regions under compression sinter faster than others where tensile stresses are predominant. Contrary, the tip of the tooth has only reached 97% relative density at that time, but at the end of the process this region is completely dense as well. The last stage of the sinter forming is fairly slow, as the component has reached "full" density in most areas and the plastic deformation can only take place by creep mechanisms. The simulation predicts a nearly homogeneous density in entire part after 180 min.

6. Summary and concluding remarks

Sinter forming is a promising technology for the fabrication of advanced ceramic components. This process combines shaping and sintering in one step and mechanical finishing can be avoided in many cases. Due to load application during sintering, dense components with excellent mechanical properties are obtained. Before this competitive manufacturing process is applied industrially, sinter forming must be understood well, for what modelling and FE simulation is a proper means.

Sinter forming experiments with various axial loads were performed on two types of RBAO powders in order to determine the model parameters. As the experimental results showed a non-linear stress/strain dependence a model for solid state sintering was extended by introducing terms for source controlled diffusion. Subsequently, the model was implemented as a user subroutine in the commercial FE code ABAQUS/Explicit® to study and optimize the process for complex shaped geometries as well. Model parameters were determined for both powders and lie in a physically meaningful range as far as known.

FE simulations of the performed experiments were carried out and assessed by comparison with experimental data and a good agreement of the shape of the samples and of the density evolutions were achieved. A more detailed parameter study of the friction coefficient would be necessary to underline the estimated value of $\mu = 0.1$.

The main target of this project was to find process parameters for sinter forming as an industrial application. Hence, manufacturing of a gear wheel was simulated. High densification and deformation rates were noticed at the earlier stages, when there is still a certain porosity in the part. As the final density is reached, the rate of plastic deformation decreases rapidly, which makes the further forming very difficult. Possible solutions are: First, the applied axial stress could be raised at the later stage of the process. Second, a higher dwell temperature could be applied, but this is not reasonable due to economic aspects and due to grain coarsening. Additionally, this would prevent the intended use of superalloys instead of SiC for the tooling, which are easier to manufacture. Third, the geometry of the semi-finished part could be optimized in a way that is closer to the final shape. This can be made easily by uniaxial pressing. By this means, a significant reduction of the sinter forming time can be reached, especially, when components are inserted and demoulded at high temperatures.

Acknowledgements

We wish to acknowledge financial support of Deutsche Forschungsgemeinschaft through grant number KR 1729/2-1 and the Advanced Ceramics Group at the TU Hamburg-Harburg for providing the samples and experimental data.

References

1. Boutz, M. M. R., von Minden, C., Janssen, R. and Claussen, N., Deformation processing of reaction bonded alumina ceramics. *Mater. Sci. Eng. A*, 1997, **233**, 155–166.
2. Claussen, N., Janssen, R. and Holz, D., reaction bonding of aluminium oxide. *J. Ceram. Soc. Jpn.*, 1995, **103**, 749–758.
3. Essl, F., Janssen, R. and Claussen, N., Wet milling of Al-containing powder mixtures as precursor materials for reaction bonding of alumina (RBAO) and reaction sintering of alumina–aluminide alloys (3A). *Mater. Chem. Phys.*, 1999, **61**, 69–77.
4. Suvaci, E., Simkovich, G. and Messing, G. L., The reaction-bonded aluminum oxide process: I, the effect of attrition milling on the solid-state oxidation of aluminum. *J. Am. Ceram. Soc.*, 2000, **83**, 299–305.
5. Suvaci, E., Simkovich, G. and Messing, G. L., The reaction-bonded aluminum oxide process: II, the solid-state oxidation of RBAO compacts. *J. Am. Ceram. Soc.*, 2000, **83**, 1845–1852.
6. Gaus, S. G., Harmer, M. P., Chan, H. M. and Caram, H. S., Controlled firing of reaction-bonded aluminum oxide (RBAO) ceramics: part I, continuum-model predictions. *J. Am. Ceram. Soc.*, 1999, **82**, 897–1805.
7. Gaus, S. G., Harmer, M. P., Chan, H. M. and Caram, H. S., Controlled firing of reaction-bonded aluminum oxide (RBAO) ceramics: part II, experimental results. *J. Am. Ceram. Soc.*, 1999, **82**, 909–924.
8. Ventakachari, K. R. and Raj, R., Enhancement of strength trough sinter forging. *J. Am. Ceram. Soc.*, 1987, **70**, 514–520.
9. Wakai, F., Sakaguchi, S. and Matsuno, Y., Superplasticity of yttria-stabilized tetragonal ZrO_2 polycristals. *Adv. Ceram. Mater.*, 1986, **1**, 259–263.
10. Owen, D. M. and Chokshi, A. H., Final stage free sintering and sinter forging behavior of a yttria-stabilized tetragonal zirconia. *Acta Mater.*, 1998, **46**, 719–729.
11. Kwon, O., Nordahl, C. S. and Messing, G. L., Submicrometer transparent alumina by sinter forging seeded gamma-Al_2O_3 powders. *J. Am. Ceram. Soc.*, 1995, **78**, 491–494.
12. Abouaf, M., Chenot, J. L., Raisson, G. and Baudin, P., Finite element simulation of hot isostatic pressing of metal powders. *Int. J. Numer. Methods Engng.*, 1988, **25**, 191–212.

13. Olevsky, E. A., Theory of sintering: from discrete to continuum. *Mater. Sci. Eng. R*, 1998, **23**, 41–100.
14. Riedel, H. and Svoboda, J., A theoretical study of grain coarsening in porous solids. *Acta Metall. Mater.*, 1993, **41**, 1929–1936.
15. Svoboda, J., Riedel, H. and Zipse, H., Equilibrium pore surfaces, sintering stresses and constitutive equations for the intermediate and late stages of sintering—part I: computation of equilibrium surfaces. *Acta Metall. Mater.*, 1994, **42**, 435–443.
16. Riedel, H., Zipse, H. and Svobada, J., Equilibrium pore surfaces, sintering stresses and constitutive equations for the intermediate and late stages of sintering—part II: diffusional densification and creep. *Acta Metall. Mater.*, 1994, **42**, 445–452.
17. Riedel, H., Kozák, V. and Svoboda, J., Densification and creep in the final stage of sintering. *Acta Metall. Mater.*, 1994, **42**, 3093–3103.
18. Kraft, T. and Riedel, H., Numerical simulation of solid state sintering-model and application, *J. Eur. Ceram. Soc.*, 2003, **24**, 345–361. doi: 10.1016/S0955-2219(03)00222X.
19. Riedel, H. and Blug, B., Comprehensive model for solid state sintering and its application to silicon-carbide. In *Multiscale Deformation and Fracture in Materials and Structures: The J.R. Rice 60th Anniversary Volume, Solid Mechanics and Its Application84*, ed. J. W. Rudnicki and T. J. Chuang. Kluwer Academic Publishers, Dordrecht, 2001, pp. 49–70.
20. Ashby, M. F., A first report on sintering diagrams. *Acta Metall.*, 1974, **22**, 275–289.
21. Ashby, M. F., HIP 6.0 Background reading, University of Cambridge, 1990.
22. Jagota, A. and Dawson, P. R., Micromechanical modelling of powder compacts—unit problems for sintering and traction induced deformation. *Acta Metall.*, 1988, **36**, 2551–2561, 2563–2573.
23. McMeeking, R. M. and Kuhn, L. T., A diffusional creep law for powder compacts. *Acta Metall. Mater.*, 1992, **40**, 961–969.
24. Cannon, R. M., Rhodes, W. H. and Heuer, A. H., Plastic deformation of fine-grained alumina (Al_2O_3): I interface-controlled diffusional creep. *J. Am. Ceram. Soc.*, 1980, **63**, 46–53.
25. Kim, B.-N., Hiraga, K., Morita, K. and Sakka, Y., Superplasticity in alumina enhanced by codispersion of 10% zirconia and 10% spinel particles. *Acta Mater.*, 2001, **49**, 887–895.
26. Kottada, R. S. and Chokshi, A. H., The high temperature tensile and compressive deformation characteristics of magnesia doped alumina. *Acta Mater.*, 2000, **48**, 3905–3915.
27. Berbon, M. Z. and Langdon, T. G., An examination of the flow process in superplastic yttria-stabilized tetrgonal zirconia. *Acta Mater.*, 1999, **47**, 2485–2495.
28. Burton, B., Interface reaction-controlled diffusional creep. A consideration of grain boundary dislocation climb sources. *Mater. Sci. Eng.*, 1972, **10**, 9–14.
29. Cocks, A. C. F., Interface reaction controlled creep. *Mech. Mater.*, 1992, **13**, 165–174.
30. Cannon, W. R., High Ductility in Alumina Containing Compensating Additives. In *Structure and Properties of MgO and Al2O3 Ceramics, Advances in Ceramics10*, ed. W. D. Kingery. American Ceramic Society, Columbus, Ohio, 1984, pp. 741–749.
31. Xue, L. A. and Chen, I-W., Superplastic alumina at temperatures below 1300 °C using charge-compensating dopants. *J. Am. Ceram. Soc.*, 1996, **79**, 233–238.